Transient Simulation of Resonant Cavity Enhanced Heterojunction Photodiodes

M. S. Ünlü, *Member, IEEE*, Y. Leblebici, *Member, IEEE*, S. M. Kang, *Fellow, IEEE*, and H. Morkoç, *Fellow, IEEE*

Abstract—**Transient response of heterojunction photodiodes under pulse illumination has been simulated. By solving discretized time dependent drift-diffusion and Poisson's equations, the local potential and carrier concentrations are computed at each time step. The device-level simulation is carried out by a circuit simulator in which localized carrier transport is modeled by circuit elements such as voltage controlled current sources, capacitors, and resistors. Results on conventional AlGaAs / GaAs and resonant cavity enhanced (RCE) GaAs / InGaAs heterojunction p-i-n photodiodes are presented. For a 10 × 10 μm^2 area detector, more than 40% bandwidth improvement along with a two-fold increase in the efficiency is predicted for RCE devices over optimized conventional photodiodes.**

HIGH-SPEED photodetectors are necessary elements of optical communication systems. As the performance of optical fiber links improves, higher bit rates become accessible requiring an equivalent improvement in the response speed of emitters and detectors. For very high-speed detection, p-i-n photodiodes are one of the best candidates [1]. Consequently, efforts have been underway for a better understanding of the transient behavior of p-i-n devices [2]–[4]. A novel approach was recently developed for transient modeling of semiconductor devices using a circuit simulator [5]. This transient model solves the time dependent semiconductor device equations on a one-dimensional grid and predicts the output current under arbitrary optical generation. A novel detector structure, where the absorbing region is integrated into a Fabry–Perot resonant cavity, has been demonstrated [6] and a drastic improvement in the high-speed performance has been predicted [7]. In this letter, we will discuss the bandwidth-efficiency limitations of conventional p-i-n photodiodes and the improvements offered by the resonant cavity enhanced (RCE) detection scheme.

The two major limitations on the speed of p-i-n-photodetectors are the transit time through the depletion region, and the charging/discharging time of diode capacitance [1]. Other limitations such as diffusion time and charge trapping can be minimized by detector design. The transit time τ_{tr} is directly proportional to the depletion width L and is governed by the speed of the slower carriers (holes in GaAs and related compounds). The longest time is required for the holes generated at the opposite side of the depletion region, and thus the transit time is $\tau_{tr} = L/v_h$, where v_h is the hole velocity. Transit time considerations suggest that for thinner intrinsic layers higher speed detection can be achieved, but at the expense of increased capacitance per area. Consequently, for any given detector area there is an optimum intrinsic layer thickness for the maximum bandwidth. Furthermore, the efficiency of a conventional detector with a thin absorption region is proportional to the thickness ($\eta \simeq \alpha L$, α is the absorption coefficient). As a result, the bandwidth-efficiency product ($f_{3dB} \cdot \eta$) of a conventional p-i-n photodetector is limited by its intrinsic material properties, i.e., $f_{3dB} \cdot \eta = 0.45\ \alpha v_h$ [1]. This product is roughly 27 GHz for GaAs detectors ($\alpha = 10^4\ cm^{-1}$, $v_h = 6 \times 10^6$ cm/s). With capacitance effects included, for a 10 × 10 μm^2 GaAs detector, the maximum $f_{3dB} \cdot \eta$ is 16.2 GHz at an optimum depletion width of 0.7 μm.

The RCE-detection can be employed to obtain high quantum efficiencies for very thin active layers [7]. Consequently, the bandwidth-efficiency product increases beyond the intrinsic limitation plaguing the conventional detectors. To compare conventional and RCE detectors, we have selected two heterojunction p-i-n photodiode structures. The depletion width is chosen to be 0.72 μm producing the maximum bandwidth-efficiency product condition for a 10 × 10 μm^2 conventional p-i-n diode. This selection of the depletion width favors the conventional structure since it is slightly larger than the optimum value for the RCE detector.

The conventional device which we modeled (#1) has a 0.64 μm thick, nominally depleted n^--GaAs absorbing region and $Al_{0.06}Ga_{0.94}As$ contact (or window) layers, as shown in Fig. 1(a). The AlGaAs contact layers allow for high-speed operation by removing the limitation imposed by the slow diffusion process through absorbing, but undepleted, regions. Within a wavelength range (825 nm < λ ≤ 870 nm) determined by the absorption edge of the AlGaAs and GaAs layers, photogeneration will only occur in the depleted GaAs region ($\alpha = 10^4\ cm^{-1}$) and the device speed is limited solely by the transit time of photogenerated carriers across the 0.72 μm depletion region. A small Al mole fraction was chosen to avoid large band discontinuities. The heterojunctions were graded and po-

Manuscript received August 21, 1992. M. S. Ünlü and H. Morkoç were supported by ONR under Contract N00014-92-J-1258, and Y. Leblebici and S. M. Kang were supported by NSF Grant ECD89-43166, and the Illinois Technology Challenge Grant SCCA92-82122.

M. S. Ünlü was with the Coordinated Science Laboratory, University of Illinois at Urbana-Champaign, Urbana, IL 61801. He is now with Boston University, Boston, MA 02215.

Y. Leblebici, S. M. Kang, and H. Markoç are with the Coordinated Science Laboratory, University of Illinois at Urbana-Champaign, Urbana, IL 61801.

IEEE Log Number 9204995.

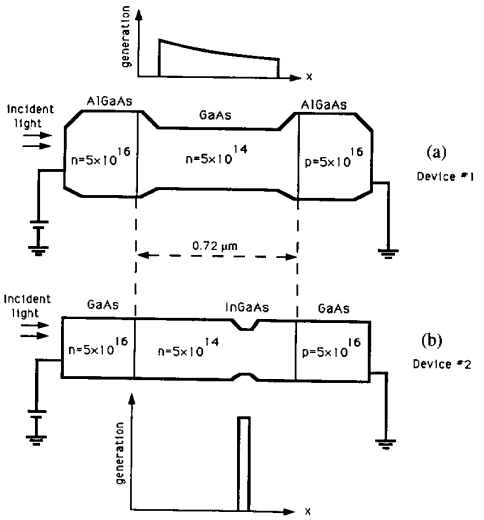

Fig. 1. The schematic flat band diagram (applied and built-in fields are not shown) of the modeled p-i-n photodiodes and the qualitative representation of the photogeneration terms. (a) Device #1: the conventional AlGaAs/GaAs p-i-n heterojunction photodiode. The photogeneration occurs in the depleted GaAs region on an exponentially decaying profile. (b) Device #2: the GaAs RCE photodiode with an InGaAs absorbing region. The generation is localized into InGaAs region.

sitioned inside the depletion region to prevent charge trapping at the heterointerface. The total band discontinuity is 75 meV, 1/3 of which is assumed to be at the valence band. For this conventional detector structure, we assume a nearly ideal anti-reflection coating ($R_1 = 0.05$) resulting in a quantum efficiency of 0.45 within the 825–875 nm wavelength range at steady state.

The RCE photodiode structure (#2) has GaAs contacts (p and n) and depletion regions [Fig. 1(b)]. A 0.08 μm thick $In_{0.07}Ga_{0.93}As$ region is placed in the depletion region extending the wavelength sensitivity spectrum of the detector to 920 nm. Within a wavelength range of 870 nm to 920 nm, only this InGaAs region absorbs ($\alpha = 10^4$ cm^{-1}) the incident light and the remainder of the detector structure is transparent. The position of the absorbing region is optimized to obtain equal transit times for electrons and holes, i.e., the distances from the absorbing layer to the n and p contact regions are inversely proportional to electron and hole velocities, respectively. The Fabry–Perot resonant cavity considered is formed by an ideal bottom mirror ($R_2 \simeq 1.0$) and a relatively high reflectivity ($R_1 = 0.7$) top mirror. The steady-state quantum efficiency of this RCE-detector is estimated at $\eta = 0.9$ at the resonant wavelength around 900 nm [7]. The photoresponse of these two structures (#1 and #2) are calculated using the one-dimensional transient simulation method we have developed [5].

Carrier transport in semiconductor devices is described by three coupled partial differential equations, i.e., Poisson's equation, the electron and hole continuity equations. We introduce three local variables defined as $x_1(j) = V(j)$, $x_2(j) = V(j) - \psi_n(j)$, and $x_3(j) = -V(j) + \psi_p(j)$ where the normalized variables V, ψ_n, and ψ_p represent the local electrostatic potential, the electron, and hole quasi-Fermi potentials. The local recombination is represented by the Shockley–Reed–Hall model in terms of these potential variables. The Scharfetter–Gummel [8] approximation has been used to express the electron and hole current densities in terms of carrier concentrations and the local potential. The change in the conduction and valence band potentials due to compositional variations is also considered as normalized potentials V_n and V_p, respectively, at every grid node. The photogeneration term is introduced as external time varying sources at nodes defined by the user allowing for spatially nonuniform generation which is essential, particularly for heterojunction devices in which the absorption coefficient varies with position. The space-discretized semiconductor equations can be modeled as three voltage controlled current sources driving lumped circuit elements such as resistors and capacitors. The local electrostatic and quasi-Fermi potentials are described by the voltages of the circuit nodes corresponding to three coupled nonlinear differential equations in time domain. Once a circuit representation for the semiconductor device is defined, a conventional circuit simulator can be used to solve these equations, i.e., evaluate the time dependent variation of electrostatic potential and carrier concentrations. Time discretization is performed within the circuit simulator according to user defined parameters. We have implemented such a device simulation using the general purpose simulation software iSMILE [9]. The circuit simulator solves for $x_i(j,t)$, $i = 1$, 2, 3, $\partial x_2(j,t)/\partial t$, and $\partial x_3(j,t)/\partial t$, which in turn gives the carrier concentrations and the local electrostatic potential as a function of time and space coordinates.

Fig. 2(a) illustrates the time evolution of the hole concentration $p(x,t)$ for Device #1 in response to a 10 ps full-width-at-half-maximum (FWHM) optical pulse (rise and fall times are 2.4 ps). The pulse magnitude and wavelength are chosen as 1×10^{20} photons/$cm^2 \cdot s$ (≈ 25 W/cm^2) and 850 nm to demonstrate the large signal capability of the model and to assure photogeneration only in the depleted GaAs region. The simulation time required for this example with 36 grid points was about 200 CPU seconds on a Sun Sparcstation 1 + . Steady state hole distribution observed at $t = 0$ is obtained by ramping the doping concentrations at the contact regions starting from a uniformly n^- structure. At $t = 2$ ps, a small precursory optical pulse is allowed to impinge first to prevent steep transitions in the carrier concentrations so that numerical convergence under large illumination is ensured.

The total current is evaluated as the sum of displacement and conduction components at the edge of the depletion region. The displacement current density J_d is calculated by summing the time derivatives of the carrier concentrations across the depletion region [3]. Fig. 2(b) illustrates the total current and its components for Device #1 under the excitation described above.

Having described the simulation tool, we can now com-

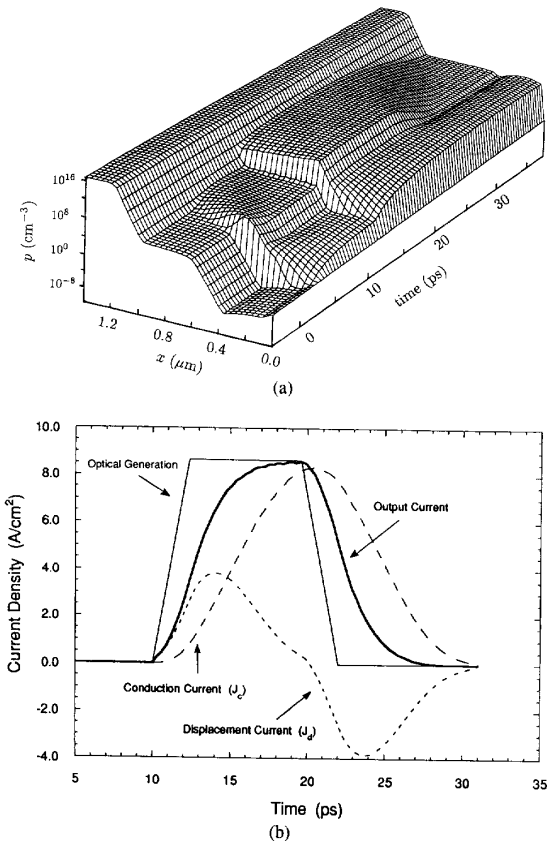

Fig. 2. (a) Simulated variation of hole concentration in the AlGaAs/GaAs p-i-n diode (Device #1) as a function of time and position when light is absorbed across the depletion region. The steady state hole distribution can be observed at $t = 0$. At $t = 2$ ps, the device is illuminated by a precursory pulse to ensure numerical convergence. The amplitude of the actual optical excitation, arriving at $t = 10$ ps, is 1×10^{20} photons/cm$^2 \cdot$ s which is six orders of magnitude larger than the precursor. (b) The short circuit current output from the device under the same pulse. The photogeneration term and different components of the current are illustrated.

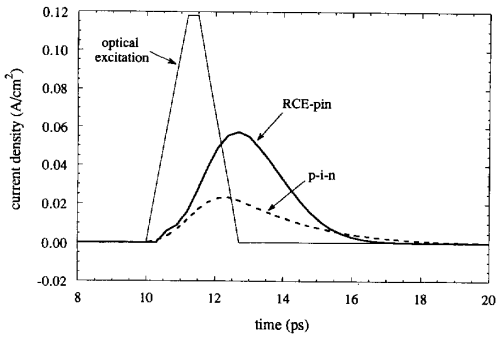

Fig. 3. The short circuit photocurrent versus time under a 1.5 ps FWHM optical excitation for AlGaAs/GaAs conventional p-i-n (Device #1, dashed line), and GaAs/InGaAs RCE p-i-n (Device #2, solid line) photodiodes. The optical excitations, $\lambda = 850$ nm (#1) and $\lambda = 900$ nm (#2), are normalized for equal photon flux for the two cases.

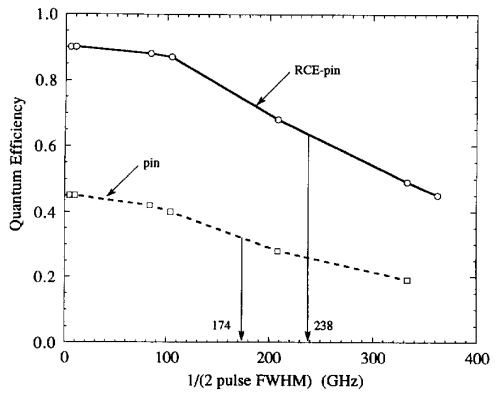

Fig. 4. The peak value of the normalized output current (quantum efficiency) versus the inverse pulse width for conventional (dashed) and RCE (solid line) p-i-n detectors. The dc quantum efficiencies are 0.45 and 0.90 for the conventional and RCE cases, respectively. The 1/FWHM values where the quantum efficiency drops of $1/\sqrt{2}$ of the steady-state value are also indicated.

pare the speed of response for conventional and RCE detectors. Within the convergence capabilities of the circuit simulator we have utilized, it is possible to calculate the output current for an optical pulse of 1.5 ps FWHM which represents a good approximation to impulse excitation. Fig. 3 shows the calculated short circuit currents for the conventional and RCE p-i-n detectors discussed earlier. The RCE-detector not only has larger current under identical optical excitation owing to the enhanced quantum efficiency, but also a faster response. Together, the bandwidth-efficiency product is doubly improved by the RCE-detection scheme. The fall times for RCE and conventional p-i-n diodes are also compared under long optical pulses to allow both devices to reach steady state. We have computed the fall time τ_f as the time it takes for the current output to drop from 90% to 10% of the steady state value. The fall time $\tau_f = 2.3$ ps for the RCE p-i-n is almost half of that for the conventional structure ($\tau_f = 4$ ps).

For a direct comparison of the bandwidths for RCE and conventional p-i-n structures, we plot the peak value of the normalized short circuit current (or overall quantum efficiency) as a function of the inverse pulse FWHM (Fig. 4). When the pulse duration is large, the output current reaches its maximum value determined by the internal quantum efficiency, i.e., $\eta = 0.45$ for conventional and $\eta = 0.9$ for RCE detectors. As the optical pulse width becomes smaller, the electrical current is unable to reach the steady state value. Although the ratio of photogenerated electron-hole pairs to the number of incident photons remains the same, the peak current decreases since the current is spread over time. The peak short circuit current drops to $1/\sqrt{2}$ of its maximum at a pulse FWHM of 2.9 and 2.1 ps for conventional and RCE p-i-n detectors, respectively. If the response under a single pulse is

taken as the measure of the bandwidth, we predict a 40% improvement for the RCE-detector over the conventional p-i-n diode. Actual bandwidth comparison can be made under sinusoidal excitation and we expect a more drastic improvement due to the large difference (> 70%) in the fall time for RCE and conventional detectors. Furthermore, if the depletion width is optimized for the RCE-detector, an additional increase in the bandwidth can also be obtained. Therefore, the bandwidth-efficiency product for RCE-detectors can be more than three times larger than that in an optimized conventional p-i-n diode.

In conclusion, a drastic improvement in the high speed performance of heterojunction photodiodes is predicted by the resonant cavity enhanced (RCE) detection scheme. The transient response of a conventional AlGaAs/GaAs and RCE GaAs/InGaAs photodiodes are accurately calculated under pulsed illumination. A three-fold improvement in bandwidth-efficiency product is estimated for RCE detectors over the optimized conventional p-i-n photodiodes. The analysis was carried out by a novel method we developed for transient simulation of heterojunction photodiodes under large signal pulse illumination. The time dependent drift-diffusion and Poisson's equations are discretized on a one-dimensional grid, and solved using a circuit simulator. Our simulation results suggest that RCE-detectors with bandwidth-efficiency products approaching 100 GHz can be realized.

ACKNOWLEDGMENT

The authors would like to thank B. Mazhari and Dr. B. Sverdlov for fruitful discussions.

REFERENCES

[1] J. E. Bowers, and C. A. Burrus, "Ultrawide-band long-wavelength p-i-n photodetectors," *J. Lightwave Technol.*, vol. **LT-5**, pp. 1339–1350, 1987.

[2] G. Lucovski, R. F., Schwarz, and R. B. Emmons, "Transit-time considerations in p-i-n diodes," *J. Appl. Phys.*, vol. **35**, pp. 622–628, 1964.

[3] M. Dentan, and B. Cremoux, "Numerical Simulation of the Nonlinear Response of a p-i-n Photodiode Under High Illumination," *J. Lightwave Technol.*, vol. 8, pp. 1137–1144, 1990.

[4] J. Hollenhorst, "Frequency response theory for multilayer photodiodes," *J. Lightwave Technol.*, vol. 8, pp. 531–537, 1990.

[5] Y. Leblebici, M. S. Ünlü, H. Morkoç, and S. M. Kang, "One dimensional transient device simulation using a direct method circuit simulator," in *Proc. IEEE Int. Symp. Circuits Syst.*, pp. 895–898, 1992.

[6] M. S. Ünlü, K. Kishino, J. I. Chyi, J. Reed, S. Noor Mohammad, and H. Morkoç, "Resonant cavity enhanced AlGaAs/GaAs heterojunction phototransistors with an intermediate InGaAs region in the collector," *Appl. Phys. Lett.*, vol. **57**, pp. 750–752, 1990.

[7] K. Kishino, M. S. Ünlü, J. I. Chyi, J. Reed, L. Arsenault, and H. Morkoç, "Resonant cavity enhanced (RCE) photodetectors," *IEEE J. Quantum Electron.*, vol. **QE-27**, pp. 2035–2034, 1991.

[8] D. L. Scharfetter and H. K. Gummel, "Large-signal analysis of a silicon read diode oscillator," *IEEE Tran. Electron. Dev.*, vol. **ED-16**, pp. 64–77, 1969.

[9] A. T. Yang, and S. M. Kang, "iSMILE: A novel circuit simulation program with emphasis on new device model development," in *Proc. 26th Design Automation Conf.*, pp. 630–633, 1989.

Hybrid Integration of Surface-Emitting Microlaser Chip and Planar Optics Substrate for Interconnection Applications

J. Jahns, R. A. Morgan, H. N. Nguyen, J. A. Walker, S. J. Walker, and Y. M. Wong

Abstract—**Compact packaging of optoelectronic systems using free-space light propagation is one of the major problems for interconnection applications. The hybrid integration of optoelectronic chips with planarized microoptic systems is a viable technique to solve this problem. We report the bonding of a monolithic array of surface-emitting microlasers onto a glass substrate that contains a matching array of microlenses and mirrors. The bonding was achieved by flip-chip solder bump bonding using indium as the solder material. The alignment precision is within ±2 μm. The optical substrate provides a simple interconnection scheme that routes the light from each laser to well defined output positions.**

Manuscript received September 2, 1992.

J. Jahns, J. A. Walker, and S. J. Walker are with AT&T Bell Laboratories, Crawford Corner Road, Holmdel, NJ 07733.

R. A. Morgan and Y. M. Wong are with AT&T Bell Laboratories, Solid-State Technology Center, Breinigsville, PA 18031.

H. N. Nguyen is with the Engineering Research Center, Princeton, NJ 08540.

IEEE Log Number 9204693.

THERE has been considerable interest in the use of optics as an interconnection technology at various levels of electronic systems. At the chip-to-chip level, this is motivated by the continuous drive of VLSI electronics towards increasing the speed and computing power of processor chips. This has turned the communications between chips into a bottleneck due to technical and physical limitations of the electrical interconnections [1]. The interest in optics as a solution to this communication